Quantitative transmission electron microscopy analysis of the nanocrystallization kinetics of soft magnetic alloys

R. V. Ramanujan and Y. R. Zhang
School of Materials Science and Engineering, Nanyang Technological University, Singapore, 639798
(Received 9 June 2006; revised manuscript received 13 October 2006; published 12 December 2006)

Transmission electron microscopy was used for the first time to obtain quantitative values of the diffusional crystallization kinetics of initially amorphous $Fe_{74.5}Si_{13.5}B_9Nb_3$, $Fe_{76.5}Si_{13.5}B_9Cu_1$ and $Fe_{73.5}Si_{13.5}B_9Nb_3Cu_1$ and $Fe_{77.5}Si_{13.5}Nb_3Cu_1$ (Finemet) alloys. The role of Cu and Nb alloying additions was elucidated. Contrary to some models of the crystallization process, it is demonstrated that both Nb and Cu alloying additions can influence the nucleation and growth processes. Combined additions of both Cu and Nb induce drastic reduction in crystal size to about 10 nm and 1000 times higher crystal number density. The high nucleation rate observed in the Fe-Si-B-Nb-Cu alloy was attributed to the formation of both Cu and Nb rich regions which provide a high number of heterogeneous nucleation sites, consistent with the Hampel and Pradell models, the low growth rate was consistent with the Hunziker model.

DOI: 10.1103/PhysRevB.74.224408 PACS number(s): 75.50.Kj

INTRODUCTION

The commercially important nanocrystalline soft magnetic $Fe_{73.5}Si_{13.5}B_9Nb_3Cu_1$ alloy, trade name Finemet, is used in power electronics applications owing to its excellent soft magnetic properties of high magnetization and low coercivity. These magnetic properties are obtained when the initially amorphous alloy is annealed at 550 °C for 1 h (Refs. 1 and 2) and is due to the formation of a high density of nanocrystals of the Fe-Si phase (with an average size of about 10 nm) within the initially amorphous alloy.[3,4] The combined presence of both Cu and Nb alloying elements in this alloy has been found to be essential to obtain this morphology. The magnetic anisotropy is reduced due to averaging by this high density of nanocrystals, thus low coercivity and high saturation magnetization can be simultaneously achieved. Thus the magnetic properties are critically dependent on the kinetics of the crystallization from the amorphous precursor, which yields the nanocrystalline morphology.

There have been many experimental reports on the kinetics of nanocrystallization in this alloy using differential scanning calorimetry (DSC), x-ray diffraction (XRD), Mossbauer spectroscopy (MS), x-ray synchrotron radiation, and nuclear magnetic resonance (NMR) techniques[5–10] but in spite of the obvious importance of obtaining a coherent physical model of the nanocrystallization process, no model has been so far successful in explaining this process. For example, the low value of the Avrami exponent and increase in nucleation rate with alloying observed experimentally has been modeled only in a qualitative fashion. The main reason is that direct quantitative data on the nucleation and growth kinetics has not been available so far, crystallization data has been previously obtained using highly indirect techniques and hence there is a need for direct quantitative TEM based data on crystallization kinetics. The crucial role of individual and combined additions of Cu and Nb on the crystallization kinetics has also not been quantitatively assessed previously, hence this investigation was carried out to obtain crystallization data for both Cu and Nb free alloys as well as alloys containing these elements. The alloy compositions were chosen to correspond to those relevant to Finemet alloys.

Previous models of the kinetics of primary crystallization in Finemet type alloys have largely been based on the Johnson-Mehl-Avrami-Kolmogorov[11] (JMAK) kinetic model. The JMAK model for isothermal (primary) crystallization kinetics is a modification to first-order reaction rate kinetics, in this model the rate of transformation depends linearly on the volume fraction of the remaining amorphous matrix, $1-X(t)$, with a rate constant k which is thermally activated

$$k = k_0 \exp\left(\frac{-Q}{k_B T}\right). \tag{1}$$

Here Q is the activation energy barrier to crystallization, k_B is the Boltzmann constant, and k_0 is a constant. The JMAK equation, for $X(t)$, is written in the general form

$$x = 1 - \exp[-(kt)_n n]. \tag{2}$$

Where X is the volume fraction transformed after time t, k is a nucleation and growth rate constant and the value of the Avrami exponent, n, depends on whether the transformation is interface or diffusion controlled. The value of n can be considered as the sum of n_n and n_g, corresponding to nucleation and growth processes, respectively. From an experimental determination of $X(t)$ at various temperatures, $k(T)$ was previously determined and Q_{JMA} calculated from the Arrhenius equation. Ozawa plots[12] were also used to determine that the activation energy for the overall crystallization process was 360 ± 40.1 kJ/mol.[13]

The Avrami exponent, n, assuming constant or decreasing nucleation rate and isotropic growth, lies between $3 < n < 4$ or $1.5 < n < 2.5$ for interface and diffusion controlled transformations, respectively.[14] Importantly however, as mentioned above, the assumptions of the JMAK model do not usually match experimental observations of nanocrystallization in initially amorphous iron-based alloys[6,15–18] and Avrami exponents $n < 1$ are typical. Thus the crystallization process in nanostructured iron-based alloys cannot be understood in terms of the conventional JMAK model, other mod-

els have also been proposed, as described below.

Uebele and Hermann studied, by means of three-dimensional computer simulations, the influence of nonuniform random and partially ordered distributions of nuclei on crystallization kinetics.[19] They showed that clusterlike arrangements of nuclei result in a smaller value of n compared with random homogeneous distribution of nuclei.

Hampel attributed the small Avrami exponent to Cu alloying additions, which increase the quenched-in nucleation sites, accelerating the nucleation of primary crystals; in the ideal case no energy is needed for nucleation (athermal nucleation) and n_n is zero.[16] This athermal nucleation is accompanied by thermally activated nucleation which yields n_n between zero and one. Further, in an amorphous alloy, crystal growth is inhomogeneous since the growth kinetics are dependent on the local composition. Therefore values of $n_g < 1$ may occur and $n=n_n+n_g$ can be less than 1.

On the other hand, Pradell and Barandiaran[7,20] attributed the anomalously low Avrami exponent to a soft impingement mechanism, following transient interface controlled growth and decreasing nucleation rate. Pradell[20] proposed that soft impingement, resulting from overlap of Nb concentration profiles is responsible for the anomalously low Avrami exponent. The growing crystal has a different composition from the amorphous matrix, i.e., it is a partitioning phase transformation, hence a microstructural dependence of crystal growth was introduced in the Pradell model. Normally partitioning transformations result in the presence of concentration gradients of several solutes at the interface of the crystals, the growth rate being limited by the slowest-diffusing specimen.[21] However, as crystallization proceeds, the diffusion profiles of neighboring crystals begin to overlap to an appreciable extent (soft impingement), giving rise to a further decrease in the growth rate because of the reduction in the concentration gradient.[9]

It is clear from the above that there is no consensus on the mode of crystallization and that widely different models have been proposed so far. TEM measurements will help to resolve these differences since we can make direct measurements of crystal size distribution, crystal number density, and crystalline volume fraction. TEM dark field images, bright field images, and selected area diffraction patterns were therefore used for the first time to provide a stereological evaluation of the crystallization kinetics in four alloys: initially amorphous $Fe_{77.5}Si_{13.5}B_9$, $Fe_{76.5}Si_{13.5}B_9Cu_1$ and $Fe_{74.5}Si_{13.5}B_9Nb_3$ and $Fe_{73.5}Si_{13.5}B_9Nb_3Cu_1$, providing quantitative evaluation of the crystal size distribution, crystal number density and volume fraction for each of these alloys. This study provides a quantitative assessment of the crucial role of the alloying elements Cu and Nb on the crystallization process and shows the importance of the synergetic effects of Cu and Nb in increasing the nucleation rate and decreasing the growth rate in these alloys. The physical models described above are evaluated in light of this data.

EXPERIMENTAL PROCEDURE

For quantitative studies of crystallization, electron energy loss spectrometry (EELS) was employed to measure the thickness of the TEM samples. The procedure for measuring specimen thickness within a region defined by the incident beam is to record an energy-loss spectrum and to compare the area under the zero loss peak (I_0) to the total area under the whole spectrum (I_t). The thickness (t) is given by

$$t/\mu = \ln(I_t/I_0), \tag{3}$$

where μ is the total mean free path for inelastic scattering. For materials of known composition, μ can be obtained in terms of the collection semiangle β, the incident energy E_0 and a mean energy loss E_m which depends on the chemical composition of the specimen

$$\mu = \frac{106F(E_0/E_m)}{\ln(2\beta E_0/E_m)} \tag{4}$$

the units of μ are nm, β in mrad, E_0 in keV, E_m in eV. F is a relativistic factor (0.618 for $E_0=200$ keV) defined by

$$F = \frac{1+E_0/1022}{(1+E_0/511)^2} \tag{5}$$

This approximation is valid only for $\beta < 15$ mrad. For a specimen with atomic number Z, E_m can be obtained from the approximate formula[21]

$$E_m \approx 7.6Z_{\text{eff}}^{0.36} \tag{6}$$

In the case of a compound Z_{eff} can be defined by

$$Z_{eff} = \frac{\sum_i f_i Z_i^{1.3}}{\sum_i f_i Z_i^{0.3}}, \tag{7}$$

where f_i is the atomic fraction of each element of atomic number Z_i.

The collection semiangle β is given by

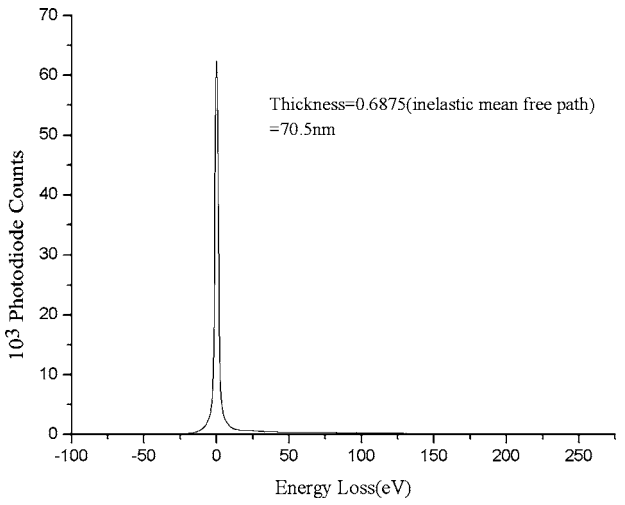

FIG. 1. Typical EELS result for a $Fe_{73.5}Si_{13.5}B_9Nb_3Cu_1$ sample heat treated at 550 °C for 1 h.

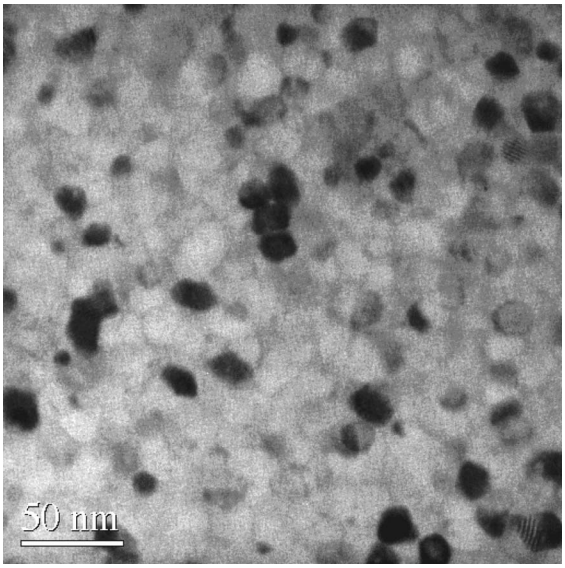

FIG. 2. BF TEM micrograph of a $Fe_{73.5}Si_{13.5}B_9Nb_3Cu_1$ sample heat treated at 500 °C for 1 h.

$$\beta = (h/h_a) \times (R/L), \tag{8}$$

where h is the distance between the projector lens crossover and the viewing screen (equal to 30 cm), h_a is the distance between the crossover and the spectrometer entrance aperture (equal to 72 cm), R is the radius of the selected entrance aperture (equal to 3 mm) and L is the camera length of the diffraction pattern visible on the microscope viewing screen (equal to 12 cm). In the present case, β=10 mrad, Z_{eff} =23.9, E_m=23.8 eV, and μ was found to be 107.3 nm.

The crystal number density and mean crystal size were measured using dark field TEM micrographs. Some crystals appear more than once in the dark field image due to the symmetry of bcc crystals, "double counting" was carefully eliminated before quantitative analysis. The micrographs show the projection of crystals between the top and bottom of the specimen, thus the crystal number density and size observed in the micrographs should be corrected for sample thickness.[22] The specimen thickness was found by the EELS technique to be typically about 100 nm, the crystal size is much smaller than this specimen thickness. The mean crystal size is given by[23]

TABLE I. Volume fraction of the Fe-Si-B-Nb-Cu alloy annealed at 500 °C for different time.

Time	Real diameter (nm) standard deviation	Number of crystals/unit volume/($m^3 \times 10^{22}$)	Volume fraction
10 min	10.1/4.21	1.43	1.09%
30 min	11.7/4.6	1.51	1.74%
1 h	11.9/4.8	2.67	2.45%
4 h	12.4/3.17	3.03	2.9%
16 h	14.8/1.49	3.35	3.68%

TABLE II. Volume fraction of the Fe-Si-B-Nb-Cu alloy annealed at 515 °C for different time.

Time	Real diameter (nm) standard deviation	Number of crystals/unit volume/($m^3 \times 10^{22}$)	Volume fraction
10 min	10.5/4.51	1.75	1.67%
30 min	12.4/5.31	2.93	2.05%
1 h	13.1/3.69	3.89	2.98%
4 h	14.4/5.27	4.23	3.6%
16 h	15.1/6.19	4.59	4.89%

$$\bar{D} = \frac{dt}{t - d + \frac{\pi A_A}{L_A}}, \tag{9}$$

where A_A is the projected area, t is the foil thickness, L_A is the perimeter density (1/nm), d is the projected diameter of the crystal, and $\bar{D}$ is the real mean diameter. The number of crystals per unit area, N_A, was determined using the line intersection technique of quantitative metallography. The number of crystals per unit volume, Nv, can then be calculated from the following relationship:

$$N_v = \frac{N_A}{t + \bar{D}}. \tag{10}$$

The volume fraction of crystal, fv, can be calculated from the measured fraction of the projected area, f_A, using the equation below

$$f_v = \frac{f_A}{1 + \frac{3t}{2D}}. \tag{11}$$

A large projected area compared with the crystal size was selected to increase the accuracy of the data.[24]

RESULTS AND DISCUSSION

Crystallization kinetics of the $Fe_{73.5}Si_{13.5}B_9Nb_3Cu_1$ (Finemet) alloy

Figure 1 shows a typical EELS result for the $Fe_{73.5}Si_{13.5}B_9Nb_3Cu_1$ (Finemet) samples heat treated at 550 °C for 60 min, thickness values were obtained from

TABLE III. Volume fraction of the Fe-Si-B-Nb-Cu alloy annealed at 530 °C for different time.

Time	Real diameter (nm) standard deviation	Number of crystals/unit volume/($m^3 \times 10^{22}$)	Volume fraction
10 min	11.8/4.76	3.24	1.89%
30 min	13.5/5.23	4.01	3.22%
1 h	13.1/6.71	4.74	3.45%
4 h	14.3/5.86	5.63	5.76%
16 h	15.4/7.11	6.25	6.41%

TABLE IV. Volume fraction of the Fe-Si-B-Nb-Cu alloy annealed at 550 °C for different time.

Time	Real diameter (nm) standard deviation	Number of crystals/unit volume/($m^3 \times 10^{22}$)	Volume fraction
10 min	13.2/5.27	4.35	3.3%
30 min	13.4/6.31	5.41	4.57%
1 h	15.5/7.3	7.79	8.24%
4 h	18.1/4.69	8.90	10.92%
16 h	21.3/6.32	8.32	9.35%

such data. Quantitative values of crystal size, density, and volume fraction of crystals as a function of annealing temperature and time obtained from TEM micrographs (e.g., Fig. 2) and a summary is presented in Tables I–IV. It can be seen from the data in the tables that crystal size, crystal number density, and volume fraction generally increased with increasing heat treatment time. Data for the crystal size distribution as a function of annealing temperature and time for the $Fe_{73.5}Si_{13.5}B_9Nb_3Cu_1$ alloy is presented in Figs. 3–6; as the annealing temperature was increased from 500 °C to 550 °C, the mean crystal size increased from 10.1 nm to 13.2 nm. Figure 7 shows the crystal volume fraction in the $Fe_{77.5}Si_{13.5}Nb_3Cu_1$ alloy at different annealing temperatures as a function of annealing time, the volume fraction increased as the annealing time and temperature was increased, it is interesting to note that crystal growth slowed down after annealing times of about 15 000 s (approx.4 h) and that the volume fraction remained roughly constant for longer annealing times.

The variation of crystal number density with heat treatment time for different annealing temperatures is plotted (Fig. 8), the crystal number density initially increased with an increase in heat treatment time but reached a constant value after about 15 000 s. As crystallization proceeded, the growth rate is initially high followed by a marked slowing down in the growth kinetics (Fig. 9).

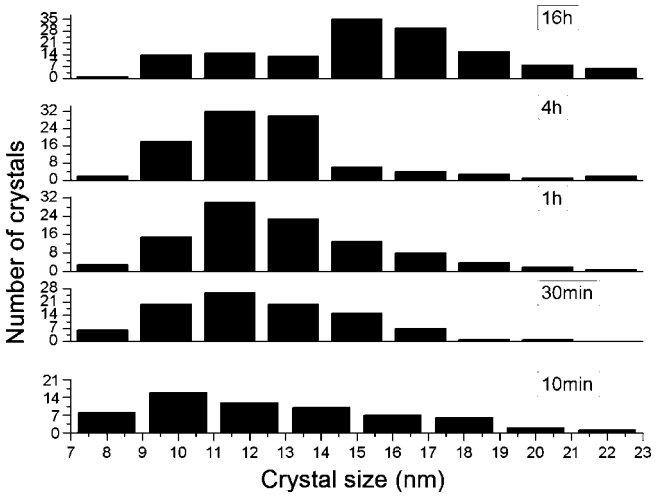

FIG. 3. Quantitative analysis of crystal size distribution in a $Fe_{73.5}Si_{13.5}B_9Nb_3Cu_1$ alloy after annealing at 500 °C.

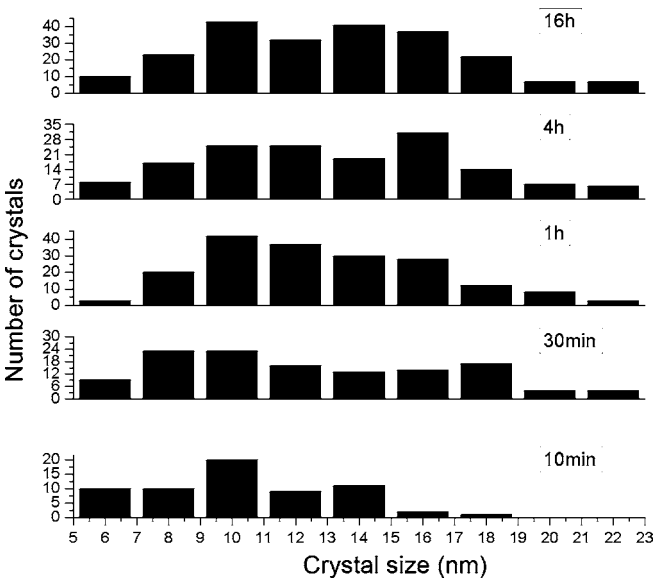

FIG. 4. Quantitative analysis of crystal size distribution as a function of annealing time in a $Fe_{73.5}Si_{13.5}B_9Nb_3Cu_1$ alloy after annealing at 515 °C.

Crystallization kinetics of $Fe_{77.5}Si_{13.5}B_9$, $Fe_{76.5}Si_{13.5}B_9Cu_1$ and $Fe_{74.5}Si_{13.5}B_9Nb_3$ alloys

The crystal size and crystal number density dependence on annealing time were similarly measured at 500 °C for the other three alloys: $Fe_{77.5}Si_{13.5}B_9$, $Fe_{76.5}Si_{13.5}B_9Cu_1$ and $Fe_{74.5}Si_{13.5}B_9Nb_3$ (Figs. 10 and 11). It can be observed that individual Cu or Nb alloying additions reduce the crystal size dramatically (from about 1500 nm to 100 nm) and also increase the crystal number density (by about three orders of magnitude), this indicates that *both* Nb and Cu alloying additions can influence the nucleation and growth processes. These experimental results shows the inadequacy of models which suggest that Cu affects only nucleation processes and that Nb only affects growth. While individual Cu and Nb

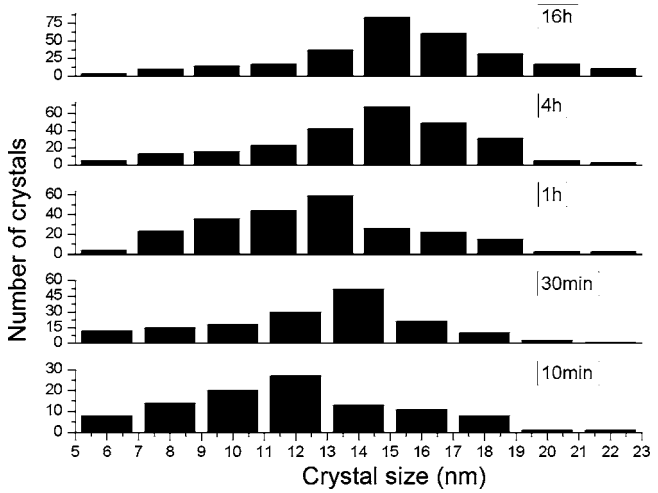

FIG. 5. Quantitative analysis of crystal size distribution as a function of annealing time in a $Fe_{73.5}Si_{13.5}B_9Nb_3Cu_1$ alloy after annealing at 530 °C.

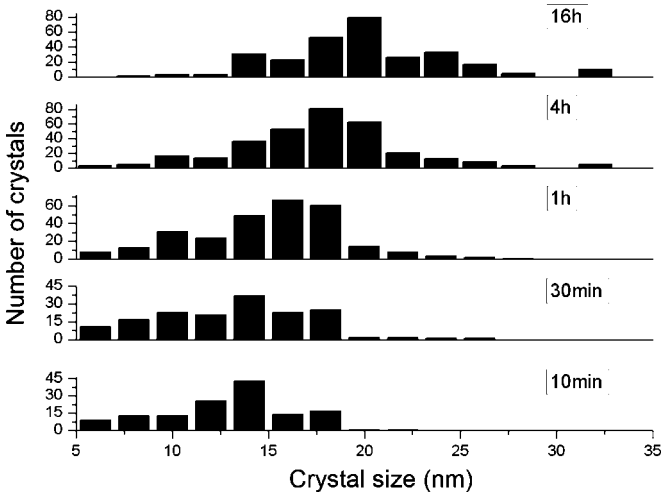

FIG. 6. Quantitative analysis of crystal size distribution as a function of annealing time in a $Fe_{73.5}Si_{13.5}B_9Nb_3Cu_1$ alloy after annealing at 550 °C.

alloying additions produce crystal sizes of about 100 nm, combined additions reduce the crystal size to 10 nm, demonstrating a synergetic effect. The nucleation rate is also increased by about 1000 times in samples with combined additions, which cannot be explained by simple additive effects. Thus, *Cu and Nb alloying additions synergetically result in nanocrystal formation.*

The Avrami exponent n and kinetic constant K for the heat treated samples for various annealing times were plotted (Fig. 12) and the values are listed in Table V, interestingly, a very low value of Avrami exponent n of about 0.25 was found. Equation (10) shows that the activation energy can be calculated by plotting ln K vs $1/T$, the activation energy was found to be 473 ± 35.2 kJ/mol, higher than that calculated by the Ozawa method (Fig. 13).[13]

Our results (Figs. 10 and 11) show that n_n less than 1 because both Cu and Nb alloying additions increase the crystal number density and reduce crystal size, perhaps by the formation of Cu and Nb rich regions formed at the initial

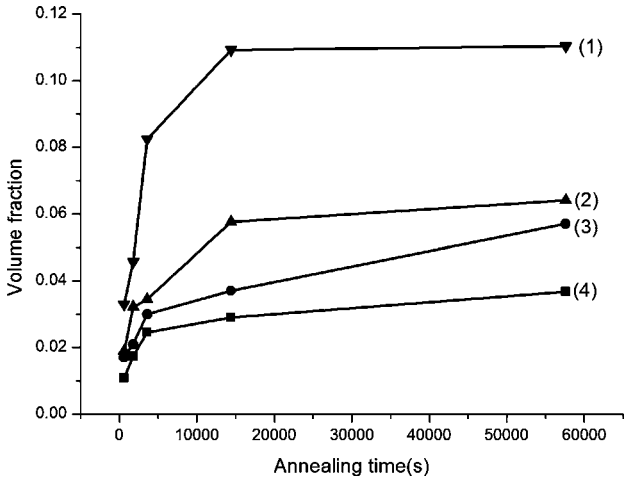

FIG. 7. Crystal volume fraction in a $Fe_{73.5}Si_{13.5}B_9Nb_3Cu_1$ alloy as a function of annealing time for annealing temperatures of (1) 550 °C, (2) 530 °C, (3) 515 °C, and (4) 500 °C.

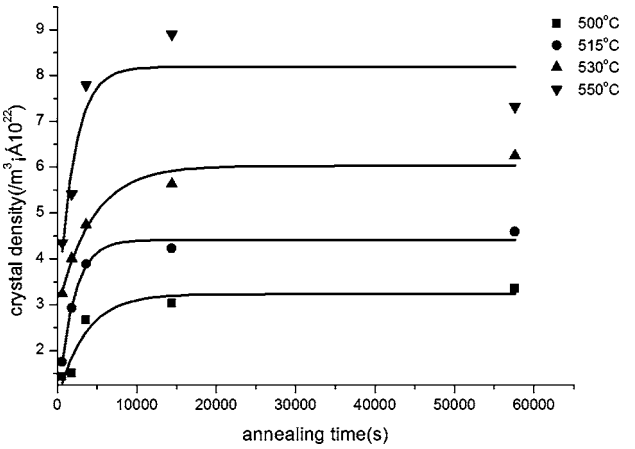

FIG. 8. The crystal number density in an annealed $Fe_{73.5}Si_{13.5}B_9Nb_3Cu_1$ alloy. Note that the number of crystal density initially rises sharply and then stabilizes at longer annealing time.

stage of crystallization. EELS maps of Cu and Nb showed that Cu and Nb rich regions served as nucleation sites for the formation of the Fe-Si crystals.[25] EDX results, previously reported by us, have also provided experimental confirmation of the repulsion of the Cu and Nb atoms, which can lead to Cu and Nb rich regions,[26] soft impingement has also been observed. The increased nucleation rate for primary crystallization in the Finemet alloy due to the high density of Cu and Nb rich nucleation sites leads to a low activation energy for nucleation, thus n_n should be less than 1, consistent with Hampel's model.[16]

The results are also consistent with Hermann's model that clusterlike arrangements of nuclei result in a smaller value of n compared with the random homogeneous (JMAK) distribution.[19] Nb rich regions serve as heterogeneous nucleation sites due to the strong attractive interaction between Si and Nb atoms, consistent with the Hunziker model which postulates that two solutes, one with atomic radius larger than the solvent and the other smaller than the solvent will tend to attract each other.[27] Local clustering associated with bcc like topological short range order lowers the configurational free energy of the nucleus,[27,28] thus the common bcc structure of Nb and Fe facilitates the formation of Nb rich regions which serve as nucleation sites for Fe-Si crystals. Thus the formation of the Cu and Nb rich regions resulted in a low Avrami value.

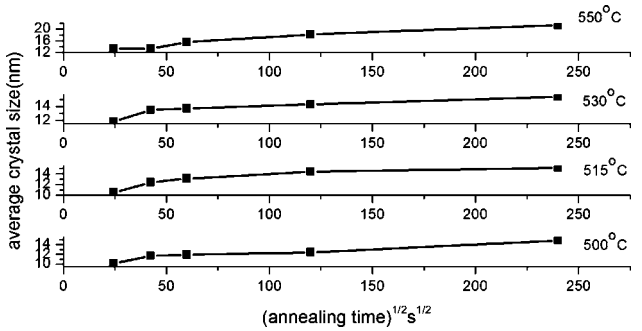

FIG. 9. The average crystal size in a $Fe_{73.5}Si_{13.5}B_9Nb_3Cu_1$ alloy as a function of annealing time for various annealing temperatures.

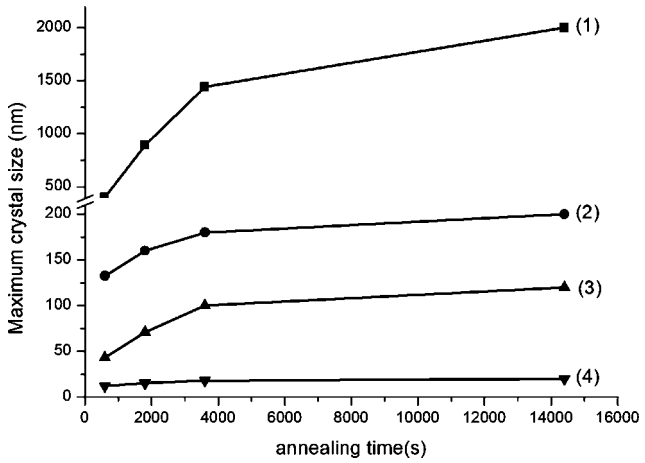

FIG. 10. Maximum crystal size as function of annealing time in Fe-Si-B, Fe-Si-B-Cu, Fe-Si-B-Nb and Fe-Si-B-Nb-Cu alloys annealed at 500 °C.

The low value of n_g has been shown from the above results to be due to the fact that both Cu and Nb alloying additions reduce the crystal size (Figs. 10 and 11). Using EDX and EELS techniques, the formation of Nb-B aggregates and soft impingement were reported earlier.[25] During growth, according to Hunziker, the interaction of solute elements can strongly influence the growth rate. The growth rate also appears to decrease due to Nb-B aggregates, consistent with Hermann's model.[29] Soft impingement due to Nb alloying additions has been also observed which hinder crystal growth, consistent with Pradell and Barandiaran's model.[7,20]

Thus it can be concluded that both Cu and Nb alloying additions influence the nucleation as well as the growth process, substantiating our previous results.[26] Individual Cu or Nb alloying additions result in higher crystal number density and smaller crystal size, however it is only with additions of *both* Cu and Nb that the smallest crystal size and highest crystal number density are observed, i.e., Cu and Nb alloying additions synergistically increase crystal number density.

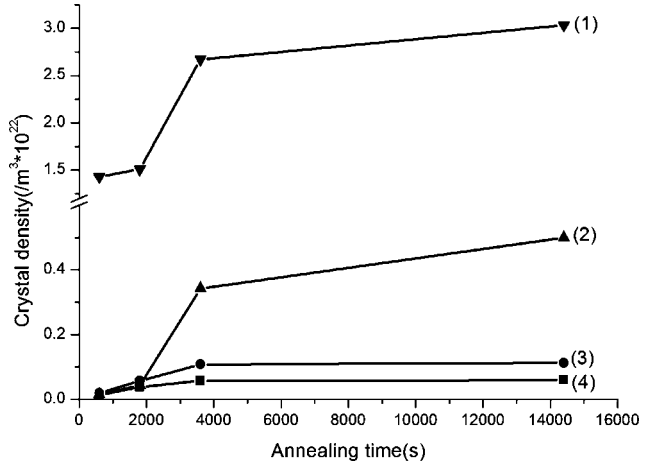

FIG. 11. The crystal number density as function of annealing time in Fe-Si-B, Fe-Si-B-Cu, Fe-Si-B-Nb and Fe-Si-B-Nb-Cu alloys annealed at 500 °C

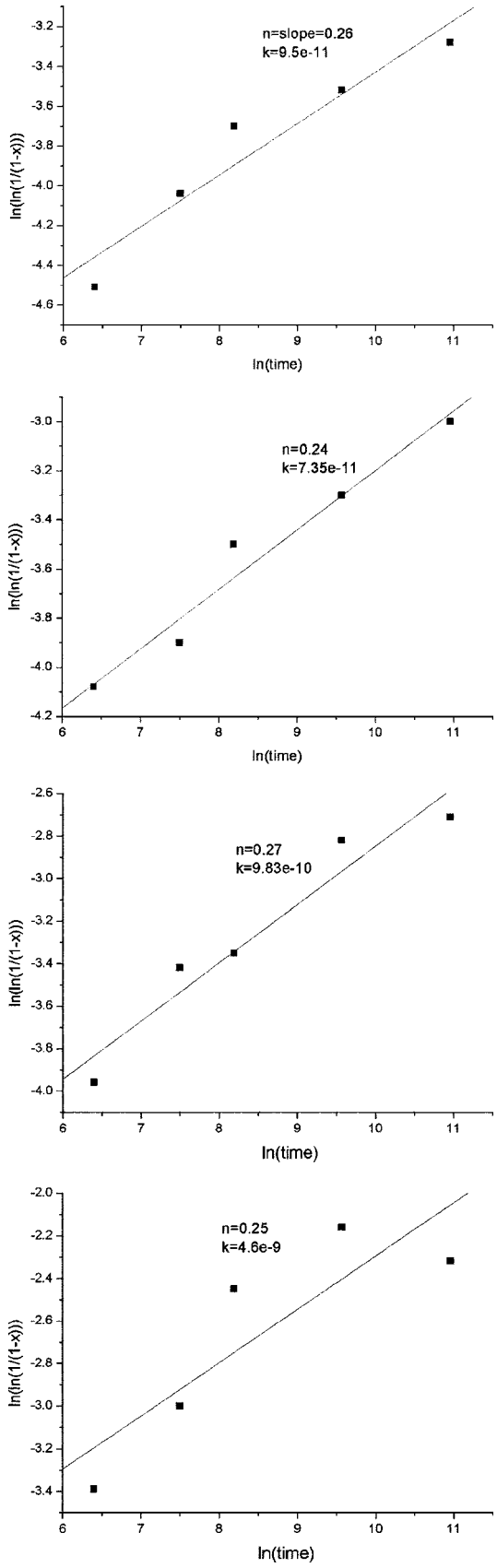

FIG. 12. JMA plot of $Fe_{77.5}Si_{13.5}Nb_3Cu_1$ alloy samples heat treated at (a) 500 °C, (b) 515 °C, (c) 530 °C, (d) 550 °C as a function of ln(time).

TABLE V. The Avrami exponent n and kinetic constant K for the annealed samples.

Temperature (°C)	Avrami exponent n	Kinetic constant K
500	0.26	9.50×10^{-11}
515	0.24	7.35×10^{-11}
530	0.27	9.83×10^{-10}
550	0.25	4.60×10^{-9}

CONCLUSIONS

A transmission electron microscopy study was carried out to quantify the kinetics of crystallization of the $Fe_{73.5}Si_{13.5}B_9Nb_3Cu_1$ (Finemet) alloy and compare it to those of the counterpart Fe-Si-B, Fe-Si-B-Nb, and Fe-Si-B-Nb-Cu alloys. Quantitative crystallization kinetics data for crystal size distribution, crystal number density, and volume fraction was obtained. The effect of individual and combined alloying additions of Cu and Nb were assessed.

(1) Individual Cu or Nb alloying additions reduce the crystal size dramatically, from 1500 nm to 100 nm and also increase the crystal number density by about three orders of magnitude.

(2) Contrary to some models of the crystallization process, it is demonstrated that both Nb and Cu alloying additions can influence the nucleation and growth processes. Combined additions of both Cu and Nb induce drastic reduction in crystal size to about 10 nm and 1000 times higher crystal number density.

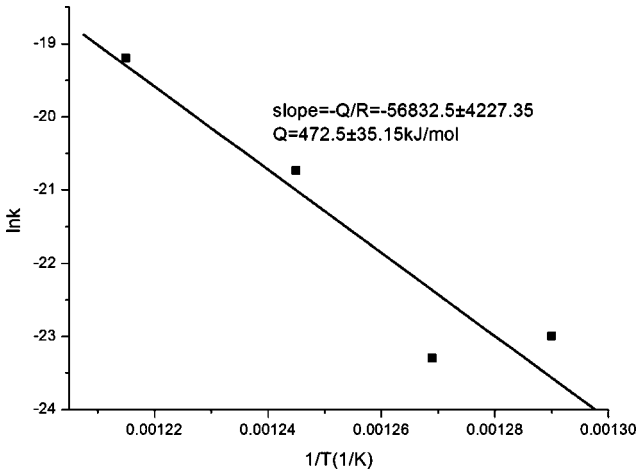

FIG. 13. Arrhenius plot of kinetic constant K for a $Fe_{77.5}Si_{13.5}Nb_3Cu_1$ alloy.

(3) The high nucleation rate observed in the Fe-Si-B-Nb-Cu alloy was attributed to the formation of both Cu and Nb rich regions which provide a high number of heterogeneous nucleation sites, consistent with the Hampel and Pradell models.

(4) The low growth rate in the Fe-Si-B-Nb-Cu alloy was attributed to Nb-B aggregates and interaction between Cu, Nb, B, Si atoms at the crystal: matrix interface, as suggested by Hunziker's model.

[1] Y. Yoshizawa, S. Oguma, and K. J. Yamauchi, J. Appl. Phys. **64**, 6044 (1988).
[2] Y. Yoshizawa, K. Yamauchi, T. Yamane, and H. Sugihara, J. Appl. Phys. **64**, 6047 (1988).
[3] G. Herzer, IEEE Trans. Magn. **26**, 1397 (1990).
[4] K. Hono, D. H. Ping, M. Ohnuma, and H. Onodera, Acta Mater. **47**, 997 (1999).
[5] F. Alves, F. Simona, and O. Hubert, Mater. Sci. Eng., A **375**, 1011 (2004).
[6] E. Illekova, Thermochim. Acta **387**, 47 (2002).
[7] J. M. Barandiaran, I. Telleria, J. S. Garitaonand, and H. A. Davies, J. Non-Cryst. Solids **329**, 57 (2003).
[8] J. M. Borrego, C. F. Conde, M. Millb, A. Conde, M. J. Caphan, and J. L. Joulaud, Nanostruct. Mater. **10**, 575 (1998).
[9] N. Ciavaguera, T. Pradell, J. Zhu, and M. T. Clavaguera-Mora, Nanostruct. Mater. **6**, 453 (1995).
[10] C. F. Barbatti, E. H. C. P Sinnecker, R. S. Sarthour, and A. P. Guimaraes, J. Alloys Compd. **369**, 136 (2004).
[11] M. Teresa, C. Mora, N. Clavaguera, D. Crespo, and T. Pradell, Prog. Mater. Sci. **47**, 559 (2002).
[12] T. Ozawa, J. Therm. Anal. **23**, 01 (1970).
[13] Y. R. Zhang and R. V. Ramanujan, Thin Solid Films **505**, 97 (2005).
[14] H. Hermann, A. Heinemann, N. Mattern, and A. Wiedenmann, Europhys. Lett. **51**, 127 (2000).
[15] N. Lecaude and J. C. Perron, *Materials Science Forum* (USA: Trans Tech Publ, 1998), Vol. 269.
[16] G. Hampel, A. Pundt, and J. Hesse, J. Phys.: Condens. Matter **43**, 195 (1992).
[17] A. Cserei, J. Jiang, F. Aubertin, and U. Gonser, J. Mater. Sci. **29**, 1213 (1994).
[18] N. Lecaude and J. C. Perron, J. Magn. Magn. Mater. **160**, 263 (1996).
[19] P. Uebele and H. Hermann, Modell. Simul. Mater. Sci. Eng. **4**, 203 (1996).
[20] T. Pradell, D. Crespoz, N. Clavaguerax, and M. T. Clavaguera-Morak, J. Phys.: Condens. Matter **10**, 3833 (1998).
[21] T. Malis, S. Cheng, and R. F. Egerton, J. Electron Microsc. Tech. **8**, 193 (1988).
[22] P. Hirsch, A. Howie, R. B. Nicholson, D. W. Pashley, and M. J. Whelan, (Robert E. Krieger Publishing Co., Huntington, New York, 1977).
[23] J. Wosik, B. Dubiel, A. Kruk, H. J. Penkalla, F. Schubert, and A. Czyrska-Filemonowicz, Mater. Charact. **46**, 119 (2001).
[24] H. J. Penkalla, J. Wosik, and A. Czyrska-Filemonowicz, Mater. Chem. Phys. **81**, 417 (2003).
[25] Y. R. Zhang, Ph.D. thesis, Nanyang Tech. Univ., Singapore, 2006.
[26] Y. R. Zhang and R. V. Ramanujan, Intermetallics **14**, 710 (2006).
[27] O. Hunziker, Acta Mater. **49**, 4191 (2001).
[28] G. Herzer and H. Warlimont, Nanostruct. Mater. **1**, 263 (1992).
[29] H. Hermann, A. Heinemann, N. Mattern, and A. Wiedenmann, Europhys. Lett. **51**, 127 (2000).